HYPERSPECTRAL, MULTISPECTRAL, AND PANCHROMATIC DATA FUSION BASED ON COUPLED NON-NEGATIVE MATRIX FACTORIZATION

Naoto Yokoya,[1] *Takehisa Yairi,*[2] *and Akira Iwasaki*[2]

[1]Department of Aeronautics and Astronautics, The University of Tokyo, Japan
[2]Research Center for Advanced Science and Technology, The University of Tokyo, Japan

ABSTRACT

Coupled non-negative matrix factorization (CNMF) is applied to hyperspectral, multispectral, and panchromatic data fusion. This unmixing based method extracts and fuses hyperspectral endmember spectra and high-spatial-resolution abundance maps using these three data. An experiment with the synthetic data simulating ALOS-3 (advanced land observing satellite 3) dataset shows that the CNMF method has a possibility to produce fused data which have both high spatial and spectral resolutions with smaller spectral distortion.

Index Terms— Data fusion, non-negative matrix factorization, spectral unmixing

1. INTRODUCTION

Panchromatic, multispectral, and hyperspectral data analysis plays an important role in remote sensing. There is always some engineering trade-off between spatial and spectral resolutions in the optical sensor design. The hyperspectral and multispectral mission named HISUI (hyperspectral imager suite) is the Japanese next-generation spaceborne radiometers [1]. The performance of the hyperspectral radiometer is 30 m ground sampling distance (GSD), 30 km swath width, and 186 spectral channels over 400-2500 nm. The performance of the multispectral radiometer is 5 m GSD, 90 km swath width, and 4 spectral channels over 450-900 nm. HISUI will be launched on advanced land observing satellite 3 (ALOS-3) of Japan aerospace exploration agency (JAXA) in FY2014. ALOS-3 also includes the high-spatial-resolution (approximately 1 m GDS) and wide-swath-width (50km) panchromatic sensor with a stereo view. Data fusion of hyperspectral, multispectral, and panchromatic data has a possibility to produce data with both higher spatial and spectral resolutions, which contribute to the accurate identification and classification of the observed materials at fine spatial resolution.

In this work, we propose coupled non-negative matrix factorization (CNMF) for hyperspectral, multispectral, and panchromatic data fusion. In recent decades, non-negative matrix factorization (NMF) has become a useful hyperspectral unmixing method [2]-[4]. Given a non-negative matrix $\mathbf{V}$, NMF looks for two non-negative matrix factors $\mathbf{W}$ and $\mathbf{H}$ such that $\mathbf{V} = \mathbf{WH}$ [5], [6]. We applied NMF to hyperspectral, multispectral, and panchromatic data fusion. Since it is based on spectral unmixing, the CNMF fused data have little spectral distortion while enhancing spatial resolution of all hyperspectral band images. The CNMF is applied to the ALOS-3 simulation dataset generated from real airborne hyperspectral data taken over vegetation areas.

2. THE CNMF ALGORITHM

The objective of this work is to estimate unobservable high-spatial-resolution hyperspectral data ($\mathbf{Z} \in \mathbb{R}^{\lambda_h \times L_p}$) from observable low-spatial-resolution hyperspectral ($\mathbf{X}_h \in \mathbb{R}^{\lambda_h \times L_h}$), multispectral ($\mathbf{X}_m \in \mathbb{R}^{\lambda_m \times L_m}$), and panchromatic data ($\mathbf{X}_p \in \mathbb{R}^{1 \times L_p}$). Here, λ_h and λ_m denote the numbers of spectral channels of hyperspectral and multispectral sensors, respectively. L_h, L_m, and L_p denote the numbers of pixels of hyperspectral, multispectral, and panchromatic images, respectively.

2.1. Observation Model

The relation between the low- and high-spatial-resolution hyperspectral data can be modeled in matrix form by

$$\mathbf{X}_h = \mathbf{Z}\mathbf{S}_h + \mathbf{N}_h, \tag{1}$$

where $\mathbf{S}_h \in \mathbb{R}^{L_p \times L_h}$ is the spatial spread transform matrix with each column vector $\{\mathbf{s}_{h,k}\}_{k=1}^{L_h}$ representing the transform from the point spread function of the high-spatial-resolution hyperspectral data to that of the k th pixel value in the low-spatial-resolution hyperspectral data. $\mathbf{N}_h$ is the residual error. Similarly, the multispectral data is modeled as

$$\mathbf{X}_m = \mathbf{R}_m\mathbf{Z}\mathbf{S}_m + \mathbf{N}_m, \tag{2}$$

where $\mathbf{R}_m \in \mathbb{R}^{\lambda_m \times \lambda_h}$ is the spectral response transform matrix with each row vector $\{\mathbf{r}_{m,i}\}_{i=1}^{\lambda_m}$ representing the transform from the spectral response function of the hyperspectral data to that of the i th band in the multispectral data. $\mathbf{S}_m \in \mathbb{R}^{L_p \times L_m}$ is the spatial spread transform matrix with each column vector $\{\mathbf{s}_{m,k}\}_{k=1}^{L_m}$ representing the

978-1-4577-2201-1/11/$26.00 ©2011 IEEE

transform from the point spread function of the high-spatial-resolution hyperspectral data to that of the k th pixel value in the multispectral data. $\mathbf{N}_m$ denotes the residual error. The panchromatic data is also modeled as

$$\mathbf{X}_p = \mathbf{R}_p\mathbf{Z} + \mathbf{N}_p, \tag{3}$$

where $\mathbf{R}_p \in \mathbb{R}^{1\times\lambda_h}$ is the spectral response transform vector which represents the transform from the spectral response function of the hyperspectral data to that of the panchromatic data. $\mathbf{N}_p$ denotes the residual error. In the simulation of this work with synthetic data, $\mathbf{S}_h$, $\mathbf{S}_m$, $\mathbf{R}_m$, and $\mathbf{R}_p$ are given.

For real data, $\mathbf{S}_h$ and $\mathbf{S}_m$ can be determined by image registrations and estimation of point spread functions. $\mathbf{R}_m$ and $\mathbf{R}_p$ can be also derived from radiometric calibration to obtain spectral response functions.

2.2. Coupled NMF Unmixing

With the linear spectral mixture assumption, $\mathbf{X}_h$, $\mathbf{X}_m$ and $\mathbf{X}_p$ are expressed as follows:

$$\mathbf{X}_h = \mathbf{W}_h\mathbf{H}_h + \mathbf{E}_h, \tag{4}$$

$$\mathbf{X}_m = \mathbf{W}_m\mathbf{H}_m + \mathbf{E}_m, \tag{5}$$

$$\mathbf{X}_p = \mathbf{W}_p\mathbf{H}_p + \mathbf{E}_p. \tag{6}$$

Here, $\mathbf{W}_h \in \mathbb{R}^{\lambda_h\times D}$, $\mathbf{H}_h \in \mathbb{R}^{D\times L_h}$, and $\mathbf{E}_h \in \mathbb{R}^{\lambda_h\times L_h}$ are the endmember, abundance, and residual matrices of the low-spatial-resolution hyperspectral data, respectively. D is the number of endmember. $\mathbf{W}_m \in \mathbb{R}^{\lambda_m\times D}$, $\mathbf{H}_m \in \mathbb{R}^{D\times L_m}$, and $\mathbf{E}_m \in \mathbb{R}^{\lambda_m\times L_m}$ are those of the multispectral data. In the same way, $\mathbf{W}_p \in \mathbb{R}^{1\times D}$, $\mathbf{H}_p \in \mathbb{R}^{D\times L_p}$, and $\mathbf{E}_p \in \mathbb{R}^{1\times L_p}$ are those of the panchromatic data. It is physically reasonable to assume that the high-spatial-resolution hyperspectral data contains the same endmember spectra as the low-spatial-resolution hyperspectral data and the same abundance maps as the panchromatic data. Therefore, $\mathbf{Z}$ can be approximated as

$$\mathbf{Z} \approx \mathbf{W}_h\mathbf{H}_p. \tag{7}$$

This is the key idea of unmixing based data fusion. CNMF is composed of two steps based on NMF, i.e., 1) the unmixings of $\mathbf{X}_h$ and $\mathbf{X}_m$, and 2) the estimation of $\mathbf{H}_p$ using $\mathbf{W}_h$ and $\mathbf{H}_m$. Finally, by combining $\mathbf{W}_h$ and $\mathbf{H}_p$, the high-spatial-resolution hyperspectral data can be obtained. Other unmixing and endmember detection algorithms are also applicable for this data fusion. But, to minimize the residual errors in the spectral mixture models taking account of sensor properties, NMF is straightforward to formulate and easy to implement.

2.2.1. Unmixings of hyperspectral and multispectral data

First, $\mathbf{X}_h$ and $\mathbf{X}_m$ are alternately unmixed by NMF to estimate $\mathbf{W}_h$ and $\mathbf{H}_m$. NMF spectral unmixing is commonly performed to minimize the squared Frobenius norm of the residual matrix in the linear spectral mixture model expressed as $\|\mathbf{E}_h\|_F^2$ and $\|\mathbf{E}_m\|_F^2$ for (4) and (5), respectively. Lee and Seung proposed a multiplicative update rule that is guaranteed to converge to a locally optimal matrix factorization under the non-negative constraints of two factorized matrices. We use the multiplicative update rule for NMF unmixings of $\mathbf{X}_h$ and $\mathbf{X}_m$. From (1), (2), (4), (5), and (7), the endmember and abundance matrices are related as

$$\mathbf{H}_h \approx \mathbf{H}_m\mathbf{S}_h^*, \tag{8}$$

$$\mathbf{W}_m \approx \mathbf{R}_m\mathbf{W}_h. \tag{9}$$

$\mathbf{S}_h^* \in \mathbb{R}^{L_m\times L_h}$ is the spatial spread transform matrix with each column vector $\left\{\mathbf{s}_{h,k}^*\right\}_{k=1}^{L_h}$ representing the transform from the point spread function of the multispectral data to that of the k th pixel value in the hyperspectral data, which can be obtained from $\mathbf{S}_h$ and $\mathbf{S}_m$. $\mathbf{X}_h$ and $\mathbf{X}_m$ are alternately unmixed to estimate $\mathbf{W}_h$ and $\mathbf{H}_m$ under constraints of (8) and (9).

The CNMF algorithm starts from NMF of $\mathbf{X}_h$ to use its spectral advantage. First, with the number of endmember D set to a certain number, $\mathbf{W}_h$ is initialized by vertex component analysis (VCA) [7], which is one of the most advanced geometry based endmember extraction methods with pure pixel assumption. $\mathbf{H}_h$ is initialized with a constant value $1/D$. Next, $\mathbf{W}_h$ and $\mathbf{H}_h$ are optimized by the multiplicative update rule. However, as the initialization phase, only $\mathbf{H}_h$ is updated until convergence with $\mathbf{W}_h$ fixed. In the subsequent rounds, the value of $\mathbf{H}_h$ that is initialized by (8) is used and $\mathbf{W}_h$ is updated with $\mathbf{H}_h$ fixed until convergence to inherit the reliable abundance information obtained from NMF of $\mathbf{X}_m$.

The alternate step is NMF of $\mathbf{X}_m$. $\mathbf{W}_m$ is initialized by (9) and $\mathbf{H}_m$ is set as a constant value $1/D$. As the initialization phase, $\mathbf{H}_m$ is updated until convergence with $\mathbf{W}_m$ fixed to inherit the reliable endmember spectra obtained from NMF of $\mathbf{X}_h$. Next, $\mathbf{W}_m$ and $\mathbf{H}_m$ are optimized by the multiplicative update rule. We refer to the alternate NMF unmixings as the outer loops and the update processes in each NMF unmxing as the inner loops. As a convergence condition, we use the condition that the change ratio of cost function achieves a value below a given threshold. Considering practical use, a maximum number of iterations is set for each loop. Two parameters are set for the outer and inner loops, respectively, as different values.

2.2.2. Estimation of high-spatial-resolution abundance matrix from panchromatic data

In the last step, the high-spatial-resolution abundance matrix is estimated from the panchromatic data by NMF. Since the panchromatic data have only one band, the initial value of $\mathbf{W}_p$ and $\mathbf{H}_p$ is significantly important for the accurate NMF of $\mathbf{X}_p$. From (3), (6), and (7), $\mathbf{W}_p$ is approximated as

$$\mathbf{W}_p \approx \mathbf{R}_p\mathbf{W}_h. \tag{10}$$

We estimate $\mathbf{W}_p$ by (10) using $\mathbf{W}_h$ obtained in the previous phase. $\mathbf{H}_p$ are initialized by the spatially up-sampled matrix of $\mathbf{H}_m$ using bilinear interpolation. Only $\mathbf{H}_p$ is optimized because the panchromatic data have no spectral information. To inherit the abundance information of $\mathbf{H}_m$, we minimize the following cost function: $\|\mathbf{E}_p\|_F^2 + \alpha\|\mathbf{H}_p - \tilde{\mathbf{H}}_m\|_F^2$, where $\tilde{\mathbf{H}}_m \in \mathbb{R}^{D\times L_p}$ denotes bilinearly up-sampled $\mathbf{H}_m$ and α is a penalty parameter. The multiplicative update rule of $\mathbf{H}_p$ is given by

$$\mathbf{H}_p \leftarrow \mathbf{H}_p .* (\mathbf{W}_p{}^T \mathbf{X}_p - \alpha(\mathbf{H}_p - \tilde{\mathbf{H}}_m))./(\mathbf{W}_p{}^T \mathbf{W}_p \mathbf{H}_p), \quad (11)$$

where $(\cdot)^T$ denotes the transposition of the matrix and $.*$ and $./$ denote element-wise multiplication and division, respectively. $\mathbf{H}_p$ is optimized by (11) until convergence. Finally, the high-spatial-resolution hyperspectral data are obtained by the multiplication of $\mathbf{W}_h$ and $\mathbf{H}_p$.

3. DATA AND METRIC

The proposed data fusion technique is applied to the ALOS-3 simulation dataset generated from real airborne hyperspectral data. The image was taken over a vegetation area in Japan by the compact airborne spectrographic imager (CASI) sensor with 68 spectral bands in the 400-1060 nm region in 2008. We selected a 480×480 pixel size image with 47 bands in the 450-900 nm region and generated the panchromatic, multispectral, and low-resolution hyperspectral data by down-sampling the original hyperspectral data in the spectral, both spectral and spatial, and spatial domains, respectively.

The panchromatic data was produced with a uniform spectral response function in the 450-900 nm region. The multispectral data was produced by averaging 5×5 pixel blocks of the original high-resolution hyperspectral data with uniform spectral response functions corresponding to multispectral bands 1-4 of HISUI, which cover the 450-520, 520-600, 630-690, and 760-900 nm regions, respectively [1]. The low-resolution hyperspectral data was generated by averaging 30×30 pixel blocks of the original high-resolution hyperspectral data. In this simulation, we assume completely identical atmospheric and illumination conditions between the three sensors.

We evaluate the spatial and spectral qualities of the fused data compared with the original data using the peak signal-to-noise ratio (PSNR) and the spectral angle error (SAE), respectively. The PSNR of the *i* th band is defined by

$$\mathrm{PSNR}_i = 10 \cdot \log_{10}\left(\frac{max_i^2}{\Sigma_{k=1}^{L_p}(\mathbf{Z} - \mathbf{W}_h\mathbf{H}_p)_{i,k}^2 / L_p}\right), \quad (12)$$

where max_i is the maximum pixel value in the *i* th band image. The SAE of each pixel is defined as an angle in λ_h spectral dimensions.

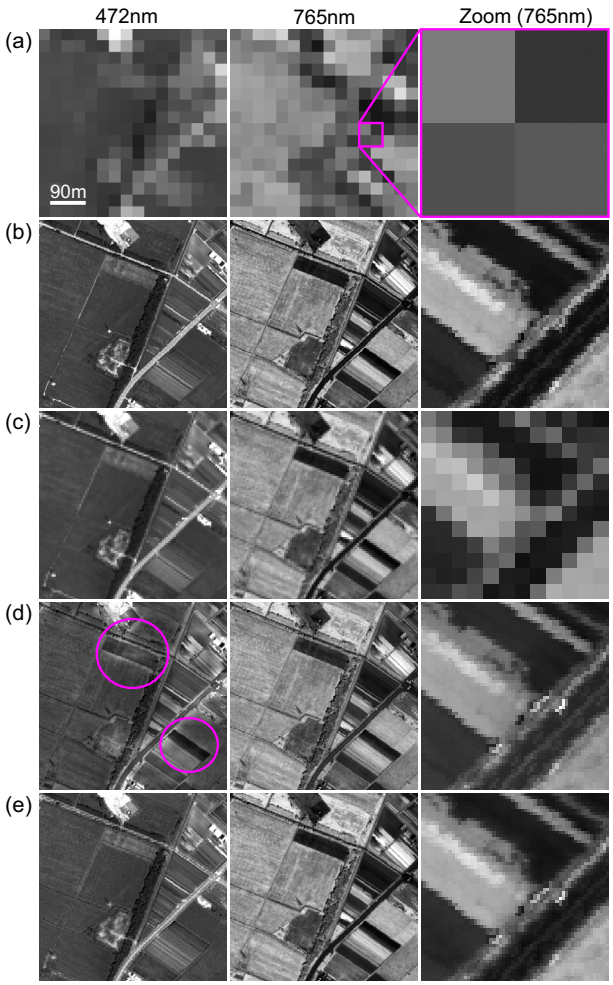

Fig. 1. 472 nm, 765 nm, and 765 nm zoomed images of (a) low-spatial-resolution hyperspectral, (b) original, (c) HM, (d) HP, and (e) HMP data.

4. RESULTS AND DISCUSSION

We compare the quality of three fused data produced by CNMF, i.e., the hyperspectral and multispectral (HM), hyperspectral and panchromatic (HP), and hyperspectral, multispectral, and panchromatic (HMP) fused data. HM is obtained in the first phase of CNMF. HP can be produced in the second phase of CNMF substituting $\mathbf{H}_h$ for $\mathbf{H}_m$ in the initialization of $\mathbf{H}_p$. Fig. 1 shows the comparison between the low-spatial-resolution hyperspectral (HS), the original, and the three fused data in the 472 nm and 765 nm regions. In the two band images, HMP is most similar to the original image regarding high spatial resolution. In the 765 nm band image, HP seems to be comparable with HMP. However, in the 472 nm band image, the reflectance values are reversed in many areas. This indicates that it is difficult to estimate abundance maps with high spatial resolution (1 m) from those with low spatial resolution (30 m).

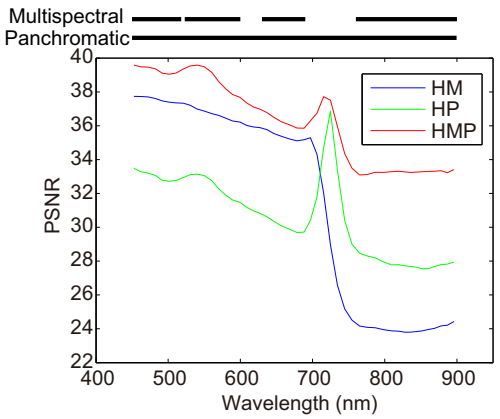

Fig. 2. PSNR of HM, HP, and HMP fused data.

Fig. 2 shows the PSNR of the three fused data. HMP outperforms HM and HP in all spectral channels. This proves that both multispectral and panchromatic data contribute to better estimation of the high-spatial-resolution hyperspectral data. Fig. 3 shows the histograms of SAE and the SAE distribution maps. HP shows large spectral distortion due to the lack of spectral information in the panchromatic data. The result that HM has less spectral distortion than HP means that the multispectral data are useful for resolution enhancement of the low-spatial-resolution hyperspectral data while keeping the spectral distortions small. HMP is thought to be comparable with HM because the panchromatic data do not contribute to the improvement of spectral quality. As shown in the SAE distribution map of HMP, SAE values are small in almost all vegetation areas and spectral distortions occur in non-vegetation area. The reason is as follows. Endmember matrix ($\mathbf{W}_h$) mainly contains vegetation spectra because the low-spatial-resolution hyperspectral data has a large coverage of vegetation area whose spectra is highly mixed. Therefore, it is difficult to linearly combine the endmembers to represent the spectra of non-vegetation materials. If we can estimate more accurate endmember spectra in the first step of CNMF, the mitigation of spectral distortions may be possible.

5. CONCLUSION

We proposed the CNMF algorithm for the fusion of panchromatic, multispectral, and hyperspectral data. First, the multispectral and hyperspectral data are alternately unmixed into the endmember and abundance matrices by NMF with the relation between sensor properties used for the constraints. Next, the high-spatial-resolution abundance maps are estimated from the panchromatic data using the hyperspectral endmember and multispectral abundance matrices. Finally, the high-spatial-resolution hyperspectral data is obtained by multiplication of the hyperspectral endmember and high-spatial-resolution abundance matrices. Owing to an algorithm based on unmixing, the CNMF method has a possibility to extract and fuse all spectral and spatial information contained in the three data. It is applicable for the high-order data product of the ALOS-3 dataset.

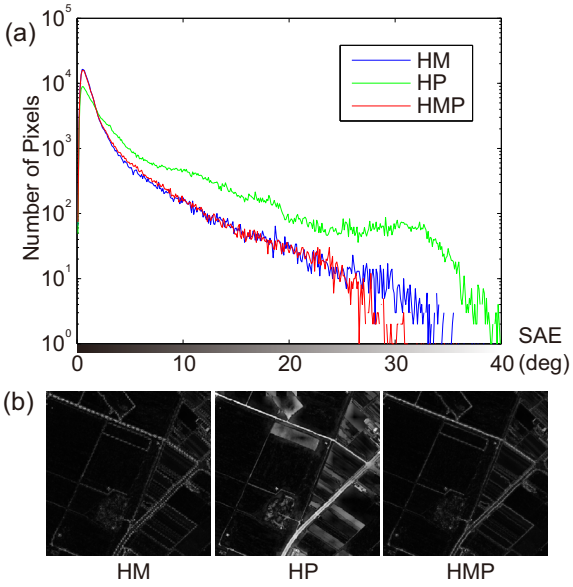

Fig. 3. (a) Histograms of SAE and (b) SAE distribution maps

6. ACKNOWLEDGMENT

The authors would like to acknowledge ERSDAC who provided CASI data.

7. REFERENCES

[1] N. Ohgi, A. Iwasaki, T. Kawashima, and H. Inada, "Japanese hyper-multi spectral mission," in Proc. IEEE IGARSS, Hawaii, USA, 2010, pp. 3756-3759.

[2] L. Miao and H. Qi, "Endmember extraction from highly mixed data using minimum volume constrained nonnegative matrix factorization," IEEE Trans. Geosci. Remote Sens., vol. 45, no. 3, pp. 765-777, Mar. 2007.

[3] S. Jia and Y. Qian, "Constrained nonnegative matrix factorization for hyperspectral unmixing," IEEE Trans. Geosci. Remote Sens., vol. 47, no. 1, pp. 161-173, Jan. 2009.

[4] A. Huck, M. Guillaume, and J. Blanc-Talon, "Minimum dispersion constrained nonnegative matrix factorization to unmix hyperspectral data," IEEE Trans. Geosci. Remote Sens., vol. 48, no. 6, pp. 2590-2602, Jun. 2010.

[5] D. D. Lee and H. S. Seung, "Learning the parts of objects by nonnegative matrix factorization," Nature, vol. 401, pp. 788-791, Oct. 1999.

[6] D. D. Lee and H. S. Seung, "Algorithms for non-negative matrix factorization," in Proc. Conf. Adv. Neural Inf. Process. Syst., 2001, vol. 13, pp. 556-562.

[7] J. M. P. Nascimento and J. M. B. Dias, "Vertex component analysis: A fast algorithm to unmix hyperspectral data," IEEE Trans. Geosci. Remote Sens., vol. 43, no. 4, pp. 898-910, Apr. 2005.